THE JOURNAL OF
PHYSICAL CHEMISTRY C

pubs.acs.org/JPCC Article

Antiferromagnetic and Electric Polarized States in Two-Dimensional Janus Semiconductor $Fe_2Cl_3I_3$

Zhen Zhang, Jing-Yang You, Bo Gu,* and Gang Su*

Cite This: https://dx.doi.org/10.1021/acs.jpcc.0c04813 Read Online

ACCESS | Metrics & More | Article Recommendations

ABSTRACT: Two-dimensional (2D) Janus semiconductors with mirror asymmetry exhibit novel properties, such as large spin−orbit coupling (SOC) and normal piezoelectric polarization, and have attracted great interest for their potential applications. Inspired by the recently fabricated 2D ferromagnetic (FM) semiconductor CrI_3, a stable 2D (in $x-y$ plane) antiferromagnetic (AFM) Janus semiconductor $Fe_2Cl_3I_3$ with normal sublattice magnetization ($\mathbf{m}\|z$) is obtained using density functional theory calculations. By applying a tensile strain, the four magnetic states sequentially occur: AFM with $\mathbf{m}\|z$ of the sublattice, AFM with $\mathbf{m}\|xy$ of the sublattice, FM with $\mathbf{m}\|xy$, and FM with $\mathbf{m}\|z$. Such a novel magnetic phase diagram driven by strain can be well understood by the spin−spin interactions including the third nearest-neighbor hoppings with the single-ion anisotropy, in which the SOC of I atoms is found to play an essential role. In addition, the electric polarization of $Fe_2Cl_3I_3$ is maintained under strain due to the broken inversion symmetry. Our results predict the rare Janus material $Fe_2Cl_3I_3$ as an example of 2D semiconductors with both spin and charge polarizations and reveal the highly sensitive strain-controlled magnetic states and magnetization direction, which highlight the 2D magnetic Janus semiconductor as a new platform to design spintronic materials.

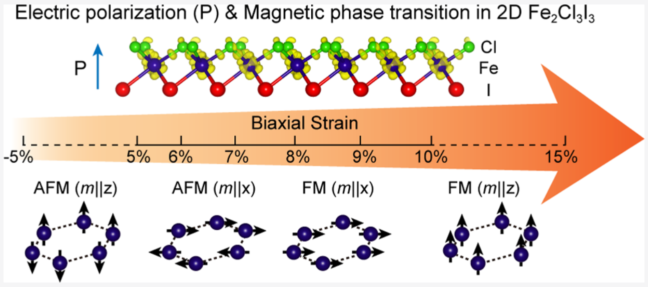

INTRODUCTION

Two-dimensional (2D) materials, such as graphene, transition metal dichalcogenides, and black phosphorus,[1−6] have attracted tremendous attention because of their excellent electrical, optical, and acoustic properties. Although much effort has been devoted to investigating 2D materials, 2D semiconductors with intrinsic magnetism are still rare.[7−12] Recently, the successful synthesis of intrinsic ferromagnetic (FM) semiconductor monolayer CrI_3[13] and bilayer $CrGeTe_3$[14] with a Curie temperature of 45 and 28 K, respectively, has attracted much attention on 2D magnetic semiconductors. However, for potential applications of these magnets in spintronics, a high Curie temperature above room temperature is highly required. In addition, a large magnetic anisotropy is needed to stabilize the magnetism in 2D systems, according to the Mermin−Wagner theorem.[15] The large magnetic anisotropy is predicted in the technetium-based 2D magnetic semiconductors.[16] A useful approach to tune magnetism and Curie temperature is by strain,[17−27] which can be realized by bending flexible substrates, elongating an elastic substrate, exploiting the thermal expansion mismatch, and so on.[28−34] The band gap can also be modified by strain. For example, a transition from the direct band gap semiconductor to a metal was proposed to occur in the MoS_2 monolayer with a tensile strain up to 15%.[35] The topological properties, such as the Weyl half-semimetal[36] and the room-temperature quantum anomalous Hall effect,[37] are recently observed in 2D FM semiconductors. Other than FM materials, antiferromagnetic (AFM) spintronics began to take a shape, because AFM materials can not only be used as assistant materials, such as pinning layers to control the magnetization direction of the adjacent FM layers, but also can work as memory materials.[38−40] Furthermore, the spin Seebeck effect in antiferromagnets MnF_2 has recently been observed in the experiment.[41] Therefore, the investigation of the FM and AFM spintronics becomes necessary and interesting.

Among various 2D materials, the 2D Janus materials are very attractive. Compared to their protypes, Janus materials have broken symmetries, and thus can induce many intriguing properties, such as large spin−orbit coupling (SOC), piezoelectricity, polarization, and so forth.[42−48] The first graphene-based Janus material was graphone, where the Dirac cone was opened with a small gap and the FM was obtained.[49] Substituting one sulfur layer with selenium in GaS, the

Received: May 28, 2020
Revised: August 11, 2020
Published: August 12, 2020

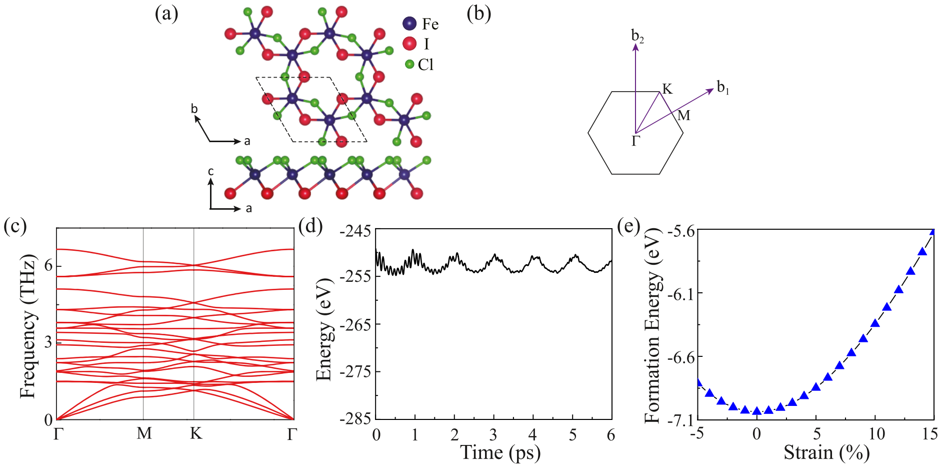

Figure 1. (a) Top and side views of the 2D Janus material $Fe_2Cl_3I_3$. (b) The first Brillouin zone with high symmetry points labeled. (c) Calculated phonon spectra. (d) MD simulations of $Fe_2Cl_3I_3$ at 300 K for 6 ps with a time step of 3 fs. (e) Formation energy as a function of applied strain.

piezoelectric coefficient in Ga_2SSe was enhanced as large as four times.[50] Recently, some magnetic Janus materials such as VSSe,[51] $Cr_2I_3X_3$,[52,53] and $V_2Cl_3I_3$[54] were theoretically studied, and they exhibited interesting properties such as large piezoelectricity and valley polarization and enhanced Curie temperatures. The 2D Janus material MoSSe,[55,56] which has been successfully synthesized recently, not only has a better hydrogen evolution reaction efficiency, but also possesses the topological and ferroelastic properties[57] compared with its protype MoS_2 monolayer.[58]

In this work, by studying 2D Janus materials $M_2Cl_3I_3$ (M = 3d transition metals) on the basis of the crystal of CrI_3, we propose a stable 2D magnetic Janus semiconductor $Fe_2Cl_3I_3$. By means of first-principles calculations, $Fe_2Cl_3I_3$ was found to be a 2D AFM semiconductor with out-of-plane magnetization ($\boldsymbol{m} \parallel z$) of the sublattice. Because of the charge redistribution caused by different electronegativity of Cl and I atoms and the broken inversion symmetry, the $Fe_2Cl_3I_3$ monolayer possesses an electrical polarization of about 0.18 e Å and a piezoelectricity of about 4.48 pm/V. By applying biaxial tensile strain up to about 15% on the $Fe_2Cl_3I_3$ monolayer, a novel phase diagram with four magnetic states is obtained: AFM with out-of-plane magnetization of the sublattice, AFM with in-plane magnetization of the sublattice, FM with in-plane magnetization, and FM with out-of-plane magnetization. The magnetic phase transition can be well understood by the spin−spin interactions with the single-ion anisotropy (SIA) term, the latter is mainly determined by the SOC of I atoms. Our results demonstrate strain-controlled magnetic phases of 2D Janus magnetic semiconductors and thus suggest a promising way to design functional materials.

COMPUTATIONAL METHODS

Our first-principles calculations were carried out with the Vienna Ab initio Simulation Package (VASP) based on the density functional theory (DFT).[59,60] The interactions between nuclei and electrons were described using the projector augmented wave method,[61] and the generalized gradient approximation (GGA) in the form proposed by Perdew, Burke, and Ernzerhof[62] was used to describe the electron exchange−correlation functional. In order to prevent the unphysical interlayer interactions, we build a 20 Å vacuum. The cutoff energy was set to be 520 eV, and the *K*-meshes for structure optimization and self-consistent calculations is 9 × 9 × 1 and 15 × 15 × 1 Γ-centered Monkhorst−Pack grid,[63] respectively. The structure optimization of atomic positions and the lattice vectors were done until the maximum force on each atom became less than 0.0001 eV/Å, and the total energy was converged to 10^{-8} eV. During the optimization, the conjugate gradient (CG) scheme were employed. To account for the correlation effects of Fe 3d electrons, the GGA + SOC + U (U = 4 eV, which is typical for 3d electrons) was used in most of our calculations, and the effect of different U values was also investigated. The phonon frequencies were obtained by the density functional perturbation theory as implemented in the PHONOPY code[64] using a 2 × 2 × 1 supercell. And the molecular dynamics (MD) simulations in the canonical (*NVT*) ensemble were performed in a 3 × 3 × 1 supercell at 300 K with a Nosé thermostat.

STRUCTURAL, MAGNETIC, AND ELECTRONIC PROPERTIES

Crystal Structures and Stability. The crystal structure of 2D Janus $Fe_2Cl_3I_3$ is shown in Figure 1a, where the Fe atoms are sandwiched by two different halogen atomic layers Cl and I. 2D $Fe_2Cl_3I_3$ with the broken inversion symmetry belongs to the $P31m$ (no. 157) space group. Each primitive cell contains one formula unit, and the Fe atoms locate in the center of the distorted octahedron consisting of three Cl atoms and three I atoms, and form a honeycomb lattice.

To examine the stability of 2D $Fe_2Cl_3I_3$, its formation energy was calculated. The formation energy is defined as $E_f = E_{Fe_2Cl_3I_3} - 2E_{Fe} - 3/2E_{Cl_2} - 3/2E_{I_2}$, where $E_{Fe_2Cl_3I_3}$ is the energy of the $Fe_2Cl_3I_3$ monolayer, E_{Fe} is the energy of bulk bcc Fe, E_{Cl_2} and E_{I_2} are the energies of the Cl_2 and I_2 molecular dimers, respectively. As shown in Table 1, the formation energy of

Table 1. Formation Energy E_f (in eV) per Primitive Cell for $Fe_2Cl_3I_3$, $FeCl_3$, and FeI_3 Monolayers Calculated by the GGA + SOC + U (U = 4 eV) Method[a]

	$Fe_2Cl_3I_3$	$FeCl_3$	FeI_3
E_f	−7.04	−8.89	−4.37

[a] Per primitive cell for $FeCl_3$ and FeI_3 is Fe_2Cl_6 and Fe_2I_6.

https://dx.doi.org/10.1021/acs.jpcc.0c04813

$Fe_2I_3Cl_3$ is between those of $FeCl_3$ and FeI_3. The negative value of $E_f = -7.04$ eV per primitive cell indicates an exothermic reaction. Inspired by the successful synthesis of MoSSe in experiments,[55,56] we propose a similar synthetic scheme to fabricate Janus $Fe_3Cl_3I_3$ as follows

$$4FeI_3 + 3Cl_2 \rightarrow 2Fe_2Cl_3I_3 + 3I_2$$

where the energy difference between products ($Fe_2Cl_3I_3$, I_2) and reactants (FeI_3, Cl_2) was −5.33 eV, and the negative value suggests the feasibility of this synthetic scheme.

The phonon spectra of the $Fe_2Cl_3I_3$ monolayer were calculated as shown in Figure 1c, where no imaginary frequency mode in the whole Brillouin zone indicates that the $Fe_2Cl_3I_3$ monolayer is dynamically stable. Moreover, after 6 ps MD simulation with a time step of 3 fs as shown in Figure 1d, no structural changes occur, and $Fe_2Cl_3I_3$ still keeps a honeycomb lattice, revealing the thermal stability of $Fe_2Cl_3I_3$. The optimized lattice constant is 6.717 Å. To investigate the mechanical property of the $Fe_2Cl_3I_3$ monolayer, the Young's modulus was calculated to be 11.4 N/m, which is much smaller than those of MoS_2 (180 N/m)[65] and graphene (342 N/m),[66,67] and MoS_2 and graphene could suffer from 11 and 13% strain, respectively. The lower Young's modulus indicates the possible applications of the $Fe_2Cl_3I_3$ monolayer under a larger tensile strain.[65] Moreover, the formation energy of $Fe_2Cl_3I_3$ as a function of applied strain, which is defined as $(a - a_0)/a_0$, is shown in Figure 1e. One may see that it changes continuously from compressed strain (−5%) to tensile strain (15%) and keeps negative values, revealing the stability of $Fe_2Cl_3I_3$ under the applied strain.

AFM Ground State. The magnetic ground state of $Fe_2Cl_3I_3$ was studied by comparing the total energy of different spin configurations: FM, Néel AFM, stripy AFM, zigzag AFM, and paramagnetic (PM) configurations. Table 2 lists the total energy per $Fe_2Cl_3I_3$ unit cell relative to the ground state. In contrast to $FeCl_3$ and FeI_3 monolayers, which possess the FM ground state as shown in Table 3, $Fe_2Cl_3I_3$ has the ground state of zigzag AFM with out-of-plane magnetization. The energy difference between the ground state and the zigzag AFM with in-plane magnetization of the sublattice is about 3.7 meV.

Table 2. Total Energy per Unit Cell for the $Fe_2Cl_3I_3$ Monolayer (in meV, Relative to the Total Energy of Zigzag AFM along z-Axis Magnetization) for Several Spin configurations of Fe Atoms Calculated by the GGA + SOC + U (U = 4 eV) Method

zigzag AFM ($m \| z$)	zigzag AFM ($m \| x$)	zigzag AFM ($m \| y$)
0.0	3.7	7.5
Néel AFM ($m \| z$)	stripy AFM ($m \| z$)	FM ($m \| z$) PM
20.1	19.3	68.9 472.1

Table 3. Magnetic Ground State, MAE (meV) Defined as the Energy Difference between the In-Plane and Out-of-Plane Magnetization Configurations, and Band Gaps (eV) for $Fe_2Cl_3I_3$, $FeCl_3$, and FeI_3, Respectively[a]

	magnetic ground state	MAE	gap
$Fe_2Cl_3I_3$	zigzag AFM ($m \| z$)	3.7	0.58
$FeCl_3$	FM ($m \| z$)	0.2	1.87
FeI_3	FM ($m \| x$)	−2.4	0.49

[a] All the above results are calculated using GGA + SOC + U (U = 4 eV).

Band Structure and Electric Polarization. The band structures as well as atom-projected density of states (DOS) of $Fe_2Cl_3I_3$ calculated using GGA + U and GGA + SOC + U (U = 4 eV) are shown in Figure 2c,d, respectively. There is a large difference between the band structures with and without SOC, where a large SOC effect can be expected in Janus materials because of the breaking of inversion symmetry. Without SOC, $Fe_2Cl_3I_3$ has an indirect band gap of about 0.83 eV. With including SOC, the band gap decreases to about 0.58 eV. The atom-projected DOS shows that the valence and conduction bands near the Fermi level are mainly contributed by I and Fe atoms, respectively. Because of the different electronegativity of Cl and I atoms, the charge redistributes. According to the Bader charge analysis, one I atom gains 0.29 e from the Fe atom, and one Cl atom gains 0.55 e from the Fe atom. Therefore, a spontaneous electric polarization along the direction perpendicular to the plane with a magnitude of 0.18 eÅ was obtained. Thus, the 2D Janus material $Fe_2Cl_3I_3$ is a rare example of the 2D semiconductors with both spin and charge polarizations.

Effects of Strain. The effects of biaxial strain from compress 5% to tensile 15% on the properties of 2D Janus material $Fe_2Cl_3I_3$ are explored. The magnetic anisotropy energy (MAE) defined as the energy difference between the states with in-plane and out-of-plane spin configurations, ΔE defined as energy difference between the FM and AFM, and the band gap and electric polarization as a function of the strain are plotted in Figure 3. From Figure 3a, it is noted that, ΔE decreases with the increase of tensile strain, and a phase transition from zigzag AFM to FM occurs with a tensile strain of 7%. Meanwhile, one can observe that MAE changes from positive to negative, and then returns to the positive value, corresponding to the change of magnetization direction from out-of-plane to in-plane, and then back to out-of-plane. The magnetic ground state changed with the strain can be briefly summarized as four steps: zigzag AFM with out-of-plane magnetization of the sublattice, zigzag AFM with in-plane magnetization of the sublattice, FM with in-plane magnetization, and FM with out-of-plane magnetization. In addition, the magnetic ground states, MAE, and band gaps for $Fe_2Cl_3I_3$, $FeCl_3$, and FeI_3 are shown in Table 3. It can be observed that the formation energy and the band gap of $Fe_2Cl_3I_3$ lie between those of $FeCl_3$ and FeI_3, while the magnetic states of these three materials are quite different. $Fe_2Cl_3I_3$ has a zigzag AFM ground state with out-of-plane sublattice magnetization, $FeCl_3$ has a FM ground state with out-of-plane magnetization, and FeI_3 has a FM ground state with in-plane magnetization. On the other hand, the band gap and electric polarization as a function of strain for $Fe_2Cl_3I_3$ are calculated using GGA + SOC + U (U = 4 eV) as shown in Figure 3b. The band gap and electric polarization preserve with the applied strain. It is interesting to note that as the strain can induce the magnetic phase transition from the zigzag AFM to FM phase, the positions of the top of the valence band and the bottom of the conduction band change under different strains as shown in Figure 4. The strain can change the overlap and hybridization of atomic orbitals, which could lead to a change of the electronic band structures. $Fe_2Cl_3I_3$ in our article shows the strain-induced magnetic phase transition between the AFM ground state and the FM ground state, and the strain-induced change of the electronic band structure between the indirect

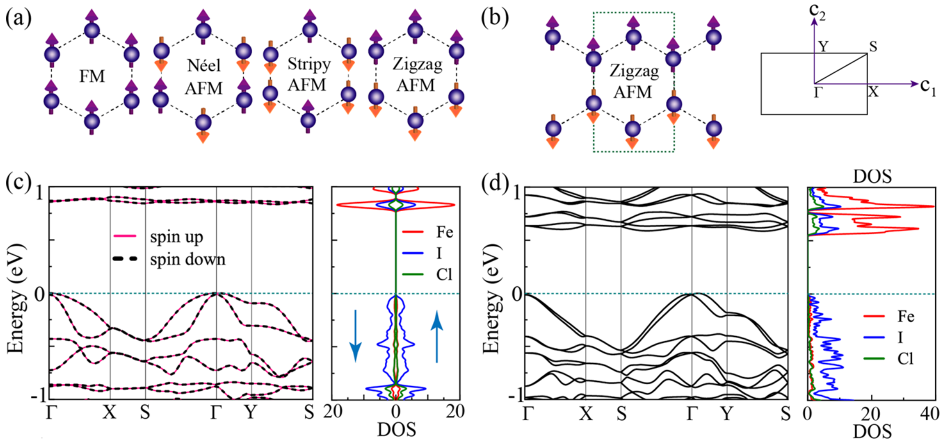

Figure 2. (a) Possible spin configurations for Fe atoms: FM, Néel AFM, stripy AFM, and zigzag AFM. (b) Unit cell for zigzag AFM spin configuration and its corresponding first Brillouin zone with high symmetry points marked. Band structure and atom-projected DOS of the zigzag AFM spin configuration for the $Fe_2Cl_3I_3$ monolayer are calculated using (c) GGA + U and (d) GGA + SOC + U (U = 4 eV).

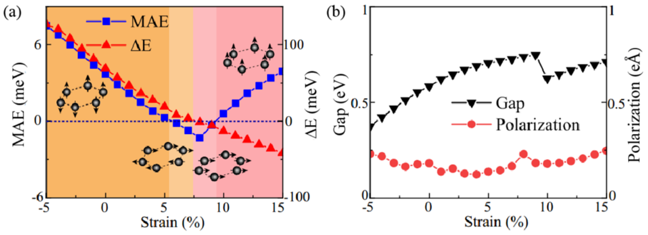

Figure 3. Strain-dependent (a) MAE, energy difference (ΔE) between FM and AFM configurations, and (b) band gap and electric polarization. A positive value of MAE indicates the out-of-plane magnetization, and a positive value of ΔE prefers the AFM ground state, otherwise the opposite. The results are calculated using the GGA + SOC + U (U = 4 eV) method.

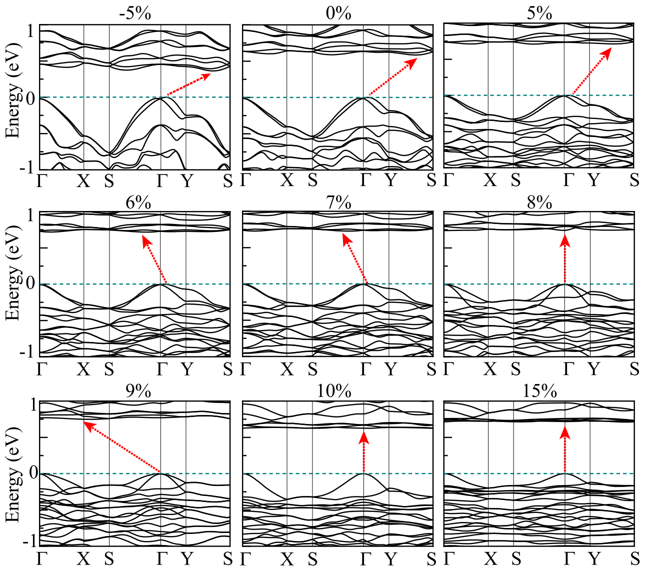

Figure 4. Band structures of Janus $Fe_2Cl_3I_3$ under different strains. The results are calculated using the GGA + SOC + U (U = 4 eV) method.

and direct band gaps. These strain-induced novel magnetic and electronic properties have not been reported in previous studies of the magnetic Janus materials VSSe,[51] $Cr_2I_3X_3$,[52,53] and $V_2Cl_3I_3$.[54] Moreover, the change of the band gap in Figure 3b shows the discontinuity at a tensile strain of 10%, where a magnetic phase transition occurs from in-plane to out-of-plane ferromagnetization.

To achieve the strain effect on 2D $Fe_2Cl_3I_3$, we could place $Fe_2Cl_3I_3$ on a 2D substrate, such as MoS_2, h-BN, and so on. Once a $Fe_2Cl_3I_3$ primitive cell matches with a 2 × 2 × 1 MoS_2 cell, whose lattice constant is about 6.36 Å, a compressive strain about 5% is applied. $Fe_2Cl_3I_3$ will retain the zigzag AFM ground state, and the magnetic anisotropy and Néel temperature will be enhanced. When we match a $Fe_2Cl_3I_3$ primitive cell with a 3 × 3 × 1 h-BN cell, there will be a tensile strain about 12%, and $Fe_2Cl_3I_3$ will change to a FM ground state.

■ THEORETICAL ANALYSIS

To better understand the strain-controlled magnetic phase transition in $Fe_2Cl_3I_3$, we employed a Hamiltonian, which can be written as

$$H = H_0 + H_1 \tag{1}$$

$$H_0 = \sum_{\langle i,j\rangle} J_1 \boldsymbol{S}_i \cdot \boldsymbol{S}_j + \sum_{\langle\langle i,j\rangle\rangle} J_2 \boldsymbol{S}_i \cdot \boldsymbol{S}_j + \sum_{\langle\langle\langle i,j\rangle\rangle\rangle} J_3 \boldsymbol{S}_i \cdot \boldsymbol{S}_j \tag{2}$$

$$H_1 = \sum_i A_{xx} S_{i,x}{}^2 + A_{yy} S_{i,y}{}^2 + A_{zz} S_{i,z}{}^2 \tag{3}$$

where H_0 includes the spin−spin interaction and H_1 contains the SIA. $\boldsymbol{S}_i$ is the spin operator at the i-th lattice site. J_1, J_2, and J_3 are the nearest-neighbor, next nearest-neighbor, and third nearest-neighbor exchange integrals, respectively. $A_{xx/yy/zz}$ represents the amplitude of SIA along the $x/y/z$ direction, and $S_{i,x/y/z}$ is the $x/y/z$ component of the i-th spin operators. Considering the spin−spin interactions are much larger than single-ion anisotropic energies, for simplicity, we ignore the SIA when we estimate J_1, J_2, and J_3 parameters based on the DFT results. Although more precise values of exchange parameters in magnetic metals can be obtained using the spin-wave stiffness method,[68] considering the complicated spin-wave behaviors of H_0 with three exchange parameters J_1, J_2, and J_3 for the magnetic semiconductor $Fe_2Cl_3I_3$, it can not be readily used to estimate these parameters by means of this method. For simplicity, we opt to use the simple method of energy mapping to estimate the exchange parameters J_1, J_2, and J_3, as reported in many previous works.[24−26,69−71] This method can also be adopted to interpret the strain-induced phase transition from AFM to FM in the 2D magnetic semiconductor $CrSiTe_3$.[69] In order to obtain J_1, J_2, and J_3, the energies corresponding to four different magnetic configurations: FM, Néel AFM, stripy AFM, and zigzag AFM were expressed as

$$
\begin{aligned}
E_{\mathrm{FM}} &= (3J_1 + 6J_2 + 3J_3)|\mathbf{S}|^2 + E_0,\\
E_{\mathrm{N\acute{e}el}} &= (-3J_1 + 6J_2 - 3J_3)|\mathbf{S}|^2 + E_0,\\
E_{\mathrm{stripy}} &= (-J_1 - 2J_2 + 3J_3)|\mathbf{S}|^2 + E_0,\\
E_{\mathrm{zigzag}} &= (J_1 - 2J_2 - 3J_3)|\mathbf{S}|^2 + E_0
\end{aligned}
\tag{4}
$$

where E_0 is the energy that is independent of spin configurations. Thus, the magnetic phase diagram with respect to J_1/J_2 and J_3/J_2 can be obtained by comparing the energies determined using eq 4 for a given set of exchange parameters, as shown in Figure 5. On the other hand, from the DFT results of $Fe_2Cl_3I_3$ with different strains, the parameters J_1, J_2, and J_3 can be estimated as marked with stars in Figure 5, where the digital numbers of each star denote the corresponding strain.

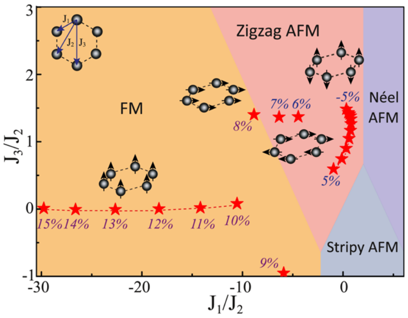

Figure 5. Magnetic phase diagram with respect to J_1/J_2 and J_3/J_2 for $Fe_2Cl_3I_3$. The DFT results with different strains are marked with stars along with the plots of the corresponding magnetic ground states.

As shown in Figure 5, $Fe_2Cl_3I_3$ locates in the zigzag AFM and FM phases. In the FM phase, the magnitude of the exchange parameter J_1 is much larger than those of J_2 and J_3, and the model Hamiltonian in eq 2 is simplified to the spin−spin interactions with nearest-neighbor coupling J_1. While in the zigzag AFM phase, both J_1, J_2, and J_3 are important. Although the jump of digital numbers in the phase diagram corresponds to four different magnetic ground states, the phase diagram is obtained from the spin−spin interactions, and cannot explain the change of the magnetization directions.

Based on the above magnetic exchange parameters J_1, J_2, and J_3, and keeping the Ising-type interactions in eq 2 for simplicity, we use Monte Carlo simulations to estimate the Curie temperature of Janus $Fe_2Cl_3I_3$ with different biaxial strain. Monte Carlo simulations are performed in a 60 × 60 × 1 2D honeycomb lattice with 10^6 steps for each temperature calculation. As shown in Figure 6, for the zigzag AFM ground states, the Néel temperature decreases from 142 to 33 K as the strain changes from −5 to 5%. When the strain changes from 10 to 15%, the Curie temperature for the corresponding FM ground states with out-of-plane magnetization increases from 65 to 193 K. As expected, the critical temperature decreases as the magnetic ground state approaches to the magnetic phase transition boundary driven by strain.

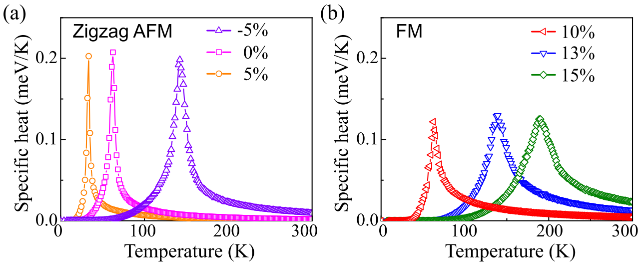

Figure 6. Specific heat as a function of temperature of Janus $Fe_2Cl_3I_3$ for (a) zigzag AFM ground state with −5, 0, and 5% strain, and (b) FM ground sate with 10, 13, and 15% strain. The results are calculated by Monte Carlo simulations based on the Ising model.

In order to understand the change of magnetization direction, that is, the sign of MAE in Figure 3a, we consider the SIA term as shown in eq 3. According to the second-order perturbation theory, the MAE caused by SIA can be described by[72,73]

$$
E_{\mathrm{SIA}} = \lambda^2 \sum_{\mathrm{o,u}} \frac{|\langle \Psi_{\mathrm{u}}|L_x|\Psi_{\mathrm{o}}\rangle|^2 - |\langle \Psi_{\mathrm{u}}|L_z|\Psi_{\mathrm{o}}\rangle|^2}{\varepsilon_{\mathrm{o}} - \varepsilon_{\mathrm{u}}}
\tag{5}
$$

where λ is the SOC constant, $L_{z/x}$ represents the angular momentum operator, Ψ_u and Ψ_o are the wavefunctions of the unoccupied and occupied states, respectively, and ε_u and ε_o are the corresponding energy levels. A positive value of E_{SIA} indicates the out-of-plane magnetization, and a negative value indicates the in-plane magnetization.

To unveil the mechanism that leads to the change of E_{SIA} with different strains, we have calculated the orbital-resolved E_{SIA}. As an example, the orbital-resolved E_{SIA} of $Fe_2Cl_3I_3$ with 8 and 15% tensile strains, which correspond to FM with magnetization along the x-axis and FM with magnetization along the z-axis ground states, respectively, was calculated as shown in Figure 7. Based on DFT calculations, the main contribution to E_{SIA} is from Fe and I atoms, and I atoms can be classified into two kinds as labeled in Figure 7a according to their different surroundings when the magnetization is along the x-axis. In the case of 8% tensile strain, as shown in Table 4, the contributions to E_{SIA} from Fe and two kinds of I atoms are −1.2, 2.5 and −4.1 meV, respectively, giving rise to a total negative E_{SIA} of −2.8 meV. It is consistent with the in-plane magnetization. For the case of 15% tensile strain, a positive value E_{SIA} of 5.3 meV is obtained, which indicates the out-of-plane magnetization. From Figure 7, one may observe that E_{SIA} mainly originates from (p_y, p_x), (p_y, p_z), and (p_z, p_x) matrix elements of I atoms. As the tensile strain increases from 8 to 15%, the sign change of E_{SIA} from I atoms gives rise to the sign change of the total E_{SIA}, and thus induces the changes in the magnetization direction.

■ EFFECT OF ELECTRONIC CORRELATION

The electronic correlation effect is important for 3d orbitals in transition-metal compounds, so our above DFT calculations are carried out with U = 4 eV. In order to examine the influence of different U values on the magnetic ground states, we have studied the magnetic sate of $Fe_2Cl_3I_3$ for the cases without strain and with 15% tensile strain with parameter U from 2 to 5 eV. As shown in Figure 8, when there is no strain applied, with the increase of the U value, although MAE increases and ΔE decreases, both the signs preserve, indicating the unchanged AFM ground state with out-of-plane magnetization of the sublattice. Similarly, the FM ground state along z-axis magnetization with 15% strain is not changed when

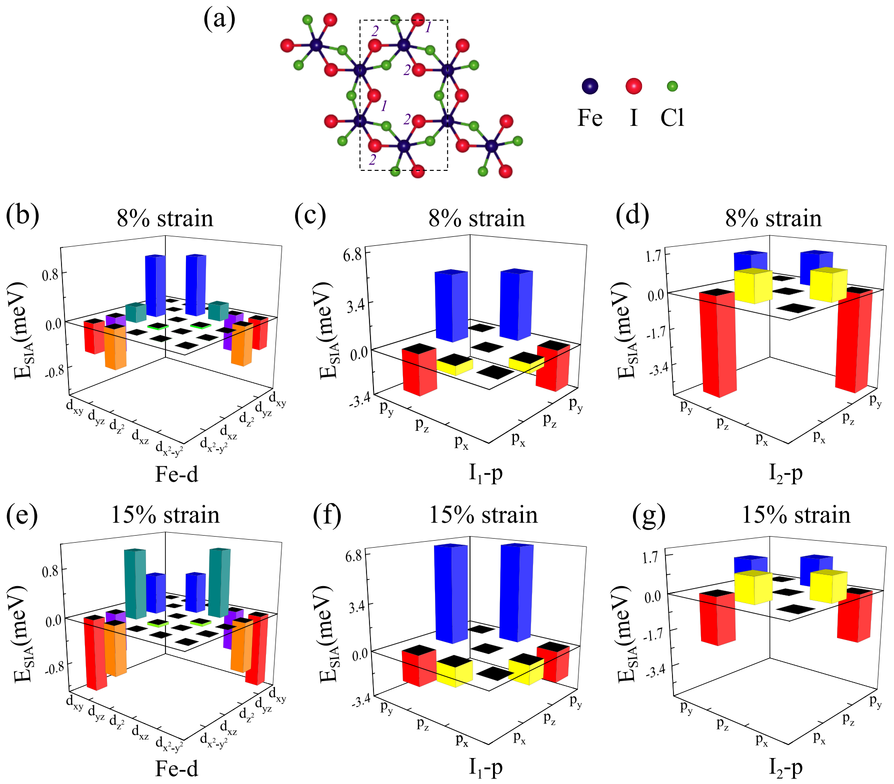

Figure 7. (a) Structure of 2D Janus materials $Fe_2Cl_3I_3$ labeled with two kinds of I atoms. Orbital-resolved SIA energy of Fe and two kinds of I atoms in the 2D Janus $Fe_2Cl_3I_3$ monolayer with (b−d) 8 and (e−g) 15% strain. Different colors represent the contributions to E_{SIA} from different d and p orbitals of Fe and I atoms.

Table 4. Orbital-Resolved Single-Ion Anisotropy Energy of Fe and Two Kinds of I Atoms (in meV) in the 2D Janus $Fe_2Cl_3I_3$ Monolayer with 8 and 15% Strain, Respectively[a]

	Fe d	I_1 p	I_2 p	total
8%	−1.2	2.5	−4.1	−2.8
15%	−2.1	6.8	0.6	4.1

[a] The results are calculated using the GGA + SOC + U (U = 4 eV) method.

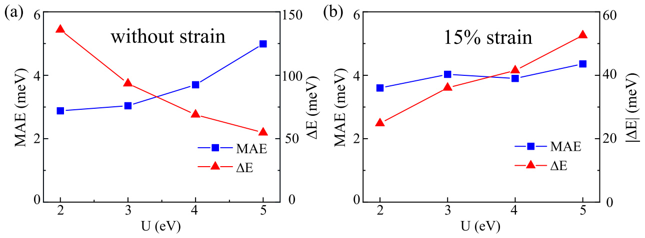

Figure 8. Electronic correlation U-dependent MAE and energy difference (ΔE) between AFM and FM configurations (a) without strain and (b) with 15% tensile strain. The results are calculated using the GGA + SOC + U method.

different U values are employed. Thus, our results for the magnetic phase transition with respect to the strain are robust against U values.

CONCLUSIONS

Using first-principles calculations, we have proposed a new 2D magnetic Janus semiconductor—$Fe_2Cl_3I_3$, which was revealed to exhibit the zigzag AFM ground state with the out-of-plane magnetic direction. In contrast to non-Janus materials, the inversion symmetry breaking usually occurs in Janus materials. This can induce the intrinsic electric polarization and enhanced spin−orbital coupling. $Fe_2Cl_3I_3$ was found to possess a spontaneous polarization along the z-axis. Furthermore, we have also investigated the effect of biaxial strain on the ground state properties of $Fe_2Cl_3I_3$, and a magnetic phase transition including the AFM−FM transition and the change of the magnetization direction was obtained. Both magnetic and electric polarization were observed in $Fe_2Cl_3I_3$ under the biaxial strain. A phase diagram based on the spin−spin interactions with the SIA term was proposed to interpret the magnetic phase transition. Our findings not only expose a new stable 2D magnetic Janus semiconductor, but also reveal the highly sensitive strain-controlled magnetic states, and thus highlight the 2D magnetic Janus semiconductor as a new platform to design spintronic materials.

AUTHOR INFORMATION

Corresponding Authors

Bo Gu − *Kavli Institute for Theoretical Sciences, and CAS Center for Excellence in Topological Quantum Computation, University of Chinese Academy of Sciences, Beijing 100190, China; Physical Science Laboratory, Huairou National Comprehensive Science Center, Beijing 101400, China*; Email: gubo@ucas.ac.cn

Gang Su − *School of Physical Sciences and Kavli Institute for Theoretical Sciences, and CAS Center for Excellence in Topological Quantum Computation, University of Chinese Academy of Sciences, Beijing 100049, China*; Email: gsu@ucas.ac.cn

Authors

Zhen Zhang − *School of Physical Sciences, University of Chinese Academy of Sciences, Beijing 100049, China;* orcid.org/0000-0002-4282-2550

Jing-Yang You − *School of Physical Sciences, University of Chinese Academy of Sciences, Beijing 100049, China;* orcid.org/0000-0003-4559-6592

Complete contact information is available at: https://pubs.acs.org/10.1021/acs.jpcc.0c04813

Author Contributions

Z.Z. and J.-Y.Y. contributed equally to this work.

Notes

The authors declare no competing financial interest.

■ ACKNOWLEDGMENTS

The authors thank Peng Fan for valuable discussions on the Monte Carlo simulations. This work was supported in part by the National Key R&D Program of China (grant no. 2018YFA0305800), the Strategic Priority Research Program of Chinese Academy of Sciences (grant no. XDB28000000), the National Natural Science Foundation of China (grant no. 11834014), and Beijing Municipal Science and Technology Commission (grant no. Z191100007219013). B.G. was also supported in part by the National Natural Science Foundation of China (grant no. Y81Z01A1A9), the Chinese Academy of Sciences (grant no. Y929013EA2), the University of Chinese Academy of Sciences (grant no. 110200M208), the Strategic Priority Research Program of Chinese Academy of Sciences (grant no. XDB33000000), and the Beijing Natural Science Foundation (grant no. Z190011).

■ REFERENCES

(1) Novoselov, K. S.; Geim, A. K.; Morozov, S. V.; Jiang, D.; Zhang, Y.; Dubonos, S. V.; Grigorieva, I. V.; Firsov, A. A. Electric field effect in atomically thin carbon films. *Science* **2004**, *306*, 666−669.

(2) Yu, A.; Ramesh, P.; Itkis, M. E.; Bekyarova, E.; Haddon, R. C. Graphite Nanoplatelet-Epoxy Composite Thermal Interface Materials. *J. Phys. Chem. C* **2007**, *111*, 7565−7569.

(3) Novoselov, K. S.; Jiang, D.; Schedin, F.; Booth, T. J.; Khotkevich, V. V.; Morozov, S. V.; Geim, A. K. Two-dimensional atomic crystals. *Proc. Natl. Acad. Sci. U.S.A.* **2005**, *102*, 10451−10453.

(4) Jin, C.; Lin, F.; Suenaga, K.; Iijima, S. Fabrication of a freestanding boron nitride single layer and its defect assignments. *Phys. Rev. Lett.* **2009**, *102*, 195505.

(5) Mak, K. F.; Lee, C.; Hone, J.; Shan, J.; Heinz, T. F. Atomically Thin MoS_2: A new direct-gap semiconductor. *Phys. Rev. Lett.* **2010**, *105*, 136805.

(6) Li, L.; Yu, Y.; Ye, G. J.; Ge, Q.; Ou, X.; Wu, H.; Feng, D.; Chen, X. H.; Zhang, Y. Black phosphorus field-effect transistors. *Nat. Nanotechnol.* **2014**, *9*, 372−377.

(7) Bonilla, M.; Kolekar, S.; Ma, Y.; Diaz, H. C.; Kalappattil, V.; Das, R.; Eggers, T.; Gutierrez, H. R.; Phan, M.-H.; Batzill, M. Strong room-temperature ferromagnetism in VSe_2 monolayers on van der Waals substrates. *Nat. Nanotechnol.* **2018**, *13*, 289−293.

(8) Wang, X.; Du, K.; Fredrik Liu, Y. Y.; Hu, P.; Zhang, J.; Zhang, Q.; Owen, M. H. S.; Lu, X.; Gan, C. K.; Sengupta, P.; et al. Raman spectroscopy of atomically thin two-dimensional magnetic iron phosphorus trisulfide ($FePS_3$) crystals. *2D Mater.* **2016**, *3*, 031009.

(9) Long, G.; Zhang, T.; Cai, X.; Hu, J.; Cho, C.-w.; Xu, S.; Shen, J.; Wu, Z.; Han, T.; Lin, J.; et al. Isolation and characterization of few-layer manganese thiophosphite. *ACS Nano* **2017**, *11*, 11330−11336.

(10) Zhou, Y.; Lu, H.; Zu, X.; Gao, F. Evidencing the existence of exciting half-metallicity in two-dimensional $TiCl_3$ and VCl_3 sheets. *Sci. Rep.* **2016**, *6*, 19407.

(11) Zheng, F.; Zhao, J.; Liu, Z.; Li, M.; Zhou, M.; Zhang, S.; Zhang, P. Tunable spin states in the two-dimensional magnet CrI_3. *Nanoscale* **2018**, *10*, 14298−14303.

(12) Ersan, F.; Vatansever, E.; Sarikurt, S.; Yüksel, Y.; Kadioglu, Y.; Ozaydin, H. D.; Aktürk, O. Ü.; Akıncı, Ü.; Aktürk, E. Exploring the electronic and magnetic properties of new metal halides from bulk to two-dimensional monolayer: RuX_3 (X=Br, I). *J. Magn. Magn. Mater.* **2019**, *476*, 111−119.

(13) Huang, B.; Clark, G.; Navarro-Moratalla, E.; Klein, D. R.; Cheng, R.; Seyler, K. L.; Zhong, D.; Schmidgall, E.; McGuire, M. A.; Cobden, D. H.; et al. Layer-dependent ferromagnetism in a van der waals crystal down to the monolayer limit. *Nature* **2017**, *546*, 270−273.

(14) Gong, C.; Li, L.; Li, Z.; Ji, H.; Stern, A.; Xia, Y.; Cao, T.; Bao, W.; Wang, C.; Wang, Y.; et al. Discovery of intrinsic ferromagnetism in two-dimensional van der waals crystals. *Nature* **2017**, *546*, 265−269.

(15) Mermin, N. D.; Wagner, H. Absence of ferromagnetism or antiferromagnetism in one- or two-dimensional isotropic Heisenberg models. *Phys. Rev. Lett.* **1966**, *17*, 1133−1136.

(16) You, J.-Y.; Zhang, Z.; Dong, X.-J.; Gu, B.; Su, G. Two-dimensional magnetic semiconductors with room curie temperatures. *Phys. Rev. Res.* **2020**, *2*, 013002.

(17) Webster, L.; Yan, J.-A. Strain-tunable magnetic anisotropy in monolayer $CrCl_3$, $CrBr_3$, and CrI_3. *Phys. Rev. B* **2018**, *98*, 144411.

(18) Huang, C.; Feng, J.; Wu, F.; Ahmed, D.; Huang, B.; Xiang, H.; Deng, K.; Kan, E. Toward intrinsic room-temperature ferromagnetism in two-dimensional semiconductors. *J. Am. Chem. Soc.* **2018**, *140*, 11519−11525.

(19) Zheng, S.; Huang, C.; Yu, T.; Xu, M.; Zhang, S.; Xu, H.; Liu, Y.; Kan, E.; Wang, Y.; Yang, G. High-temperature ferromagnetism in an Fe_3P monolayer with a large magnetic anisotropy. *J. Phys. Chem. Lett.* **2019**, *10*, 2733−2738.

(20) Dong, X.-J.; You, J.-Y.; Gu, B.; Su, G. Strain-induced room-temperature ferromagnetic semiconductors with large anomalous hall conductivity in two-dimensional $Cr_2Ge_2Se_6$. *Phys. Rev. Appl.* **2019**, *12*, 014020.

(21) Baskurt, M.; Eren, I.; Yagmurcukardes, M.; Sahin, H. Vanadium dopant- and strain-dependent magnetic properties of single-layer VI_3. *Appl. Surf. Sci.* **2020**, *508*, 144937.

(22) Ersan, F.; Sarikurt, S. Monitoring the electronic, thermal and optical properties of two-dimensional MoO_2 under strain via vibrational spectroscopies: a first-principles investigation. *Phys. Chem. Chem. Phys.* **2019**, *21*, 19904−19914.

(23) Iyikanat, F.; Yagmurcukardes, M.; Senger, R. T.; Sahin, H. Tuning electronic and magnetic properties of monolayer α-$RuCl_3$ by in-plane strain. *J. Mater. Chem. C* **2018**, *6*, 2019−2025.

(24) Sarikurt, S.; Kadioglu, Y.; Ersan, F.; Vatansever, E.; Aktürk, O. Ü.; Yüksel, Y.; Akıncı, Ü.; Aktürk, E. Electronic and magnetic properties of monolayer α-$RuCl_3$: a first-principles and monte carlo study. *Phys. Chem. Chem. Phys.* **2018**, *20*, 997−1004.

(25) Vatansever, E.; Sarikurt, S.; Ersan, F.; Kadioglu, Y.; Üzengi Aktürk, O.; Yüksel, Y.; Ataca, C.; Aktürk, E.; Akıncı, Ü. Strain effects on electronic and magnetic properties of the monolayer α-$RuCl_3$: A first-principles and monte carlo study. *J. Appl. Phys.* **2019**, *125*, 083903.

(26) Shen, Z.; Fan, X.; Yang, D.; Gong, Y.; Ma, S.; Guo, N.; Hu, Y.; Benassi, E.; Lau, W. First-principles study the single-layer transition metal trihalide $CrXSe_3$ (X = Sn, Ge, Si) as monolayer ferromagnetic semiconductor. *J. Phys.: Condens. Matter* **2019**, *32*, 085801.

(27) Wu, Z.; Yu, J.; Yuan, S. Strain-tunable magnetic and electronic properties of monolayer CrI_3. *Phys. Chem. Chem. Phys.* **2019**, *21*, 7750−7755.

(28) Conley, H. J.; Wang, B.; Ziegler, J. I.; Haglund, R. F.; Pantelides, S. T.; Bolotin, K. I. Bandgap engineering of strained monolayer and bilayer MoS_2. *Nano Lett.* **2013**, *13*, 3626−3630.

(29) He, K.; Poole, C.; Mak, K. F.; Shan, J. Experimental demonstration of continuous electronic structure tuning via strain in atomically thin MoS_2. *Nano Lett.* **2013**, *13*, 2931−2936.

(30) Wang, Y.; Cong, C.; Yang, W.; Shang, J.; Peimyoo, N.; Chen, Y.; Kang, J.; Wang, J.; Huang, W.; Yu, T. Strain-induced direct−indirect bandgap transition and phonon modulation in monolayer WS_2. *Nano Res.* **2015**, *8*, 2562−2572.

(31) Hui, Y. Y.; Liu, X.; Jie, W.; Chan, N. Y.; Hao, J.; Hsu, Y.-T.; Li, L.-J.; Guo, W.; Lau, S. P. Exceptional tunability of band energy in a compressively strained trilayer MoS_2 sheet. *ACS Nano* **2013**, *7*, 7126−7131.

(32) Plechinger, G.; Castellanos-Gomez, A.; Buscema, M.; van der Zant, H. S. J.; Steele, G. A.; Kuc, A.; Heine, T.; Schüller, C.; Korn, T. Control of biaxial strain in single-layer molybdenite using local thermal expansion of the substrate. *2D Mater* **2015**, *2*, 015006.

(33) Castellanos-Gomez, A.; Roldán, R.; Cappelluti, E.; Buscema, M.; Guinea, F.; van der Zant, H. S. J.; Steele, G. A. Local strain engineering in atomically thin MoS_2. *Nano Lett.* **2013**, *13*, 5361−5366.

(34) Roldán, R.; Castellanos-Gomez, A.; Cappelluti, E.; Guinea, F. Strain engineering in semiconducting two-dimensional crystals. *J. Phys.: Condens. Matter* **2015**, *27*, 313201.

(35) Scalise, E.; Houssa, M.; Pourtois, G.; Afanas'ev, V.; Stesmans, A. Strain-induced semiconductor to metal transition in the two-dimensional honeycomb structure of MoS_2. *Nano Res.* **2011**, *5*, 43−48.

(36) You, J.-Y.; Chen, C.; Zhang, Z.; Sheng, X.-L.; Yang, S. A.; Su, G. Two-dimensional Weyl half-semimetal and tunable quantum anomalous Hall effect. *Phys. Rev. B* **2019**, *100*, 064408.

(37) You, J.-Y.; Zhang, Z.; Gu, B.; Su, G. Two-dimensional room-temperature ferromagnetic semiconductors with quantum anomalous Hall effect. *Phys. Rev. Appl.* **2019**, *12*, 024063.

(38) Marti, X.; Fina, I.; Frontera, C.; Liu, J.; Wadley, P.; He, Q.; Paull, R. J.; Clarkson, J. D.; Kudrnovský, J.; Turek, I.; et al. Room-temperature antiferromagnetic memory resistor. *Nat. Mater.* **2014**, *13*, 367−374.

(39) Wadley, P.; Howells, B.; elezny, J.; Andrews, C.; Hills, V.; Campion, R. P.; Novak, V.; Olejnik, K.; Maccherozzi, F.; Dhesi, S. S.; et al. Electrical switching of an antiferromagnet. *Science* **2016**, *351*, 587−590.

(40) Olejník, K.; Seifert, T.; Kašpar, Z.; Novák, V.; Wadley, P.; Campion, R. P.; Baumgartner, M.; Gambardella, P.; Němec, P.; Wunderlich, J.; et al. Terahertz electrical writing speed in an antiferromagnetic memory. *Sci. Adv.* **2018**, *4*, No. eaar3566.

(41) Wu, S. M.; Zhang, W.; KC, A.; Borisov, P.; Pearson, J. E.; Jiang, J. S.; Lederman, D.; Hoffmann, A.; Bhattacharya, A. Antiferromagnetic spin seebeck effect. *Phys. Rev. Lett.* **2016**, *116*, 097204.

(42) Yang, Y.; Zhang, Y.; Ye, H.; Yu, Z.; Liu, Y.; Su, B.; Xu, W. Structural and electronic properties of 2H phase janus transition metal dichalcogenide bilayers. *Superlattices Microstruct.* **2019**, *131*, 8−14.

(43) Dong, L.; Lou, J.; Shenoy, V. B. Large in-plane and vertical piezoelectricity in Janus transition metal dichalchogenides. *ACS Nano* **2017**, *11*, 8242−8248.

(44) Guo, Y.; Zhou, S.; Bai, Y.; Zhao, J. Defects and oxidation of group-III monochalcogenide monolayers. *J. Chem. Phys.* **2017**, *147*, 104709.

(45) Cheng, Y. C.; Zhu, Z. Y.; Tahir, M.; Schwingenschlögl, U. Spin-orbit−induced spin splittings in polar transition metal dichalcogenide monolayers. *Europhys. Lett.* **2013**, *102*, 57001.

(46) Yin, W.-J.; Wen, B.; Nie, G.-Z.; Wei, X.-L.; Liu, L.-M. Tunable dipole and carrier mobility for a few layer Janus MoSSe structure. *J. Mater. Chem. C* **2018**, *6*, 1693−1700.

(47) Xu, C.; Feng, J.; Prokhorenko, S.; Nahas, Y.; Xiang, H.; Bellaiche, L. Topological spin texture in janus monolayers of the chromium trihalides $Cr(I, X)_3$. *Phys. Rev. B* **2020**, *101*, No. 060404(R).

(48) Kandemir, A.; Peeters, F. M.; Sahin, H. Monitoring the effect of asymmetrical vertical strain on Janus single layers of MoSSe via vibrational spectrum. *J. Chem. Phys.* **2018**, *149*, 084707.

(49) Zhou, J.; Wang, Q.; Sun, Q.; Chen, X. S.; Kawazoe, Y.; Jena, P. Ferromagnetism in semihydrogenated graphene sheet. *Nano Lett.* **2009**, *9*, 3867−3870.

(50) Guo, Y.; Zhou, S.; Bai, Y.; Zhao, J. Enhanced piezoelectric effect in Janus group-III chalcogenide monolayers. *Appl. Phys. Lett.* **2017**, *110*, 163102.

(51) Zhang, C.; Nie, Y.; Sanvito, S.; Du, A. First-principles prediction of a room-temperature ferromagnetic Janus VSSe monolayer with piezoelectricity, ferroelasticity, and large valley polarization. *Nano Lett.* **2019**, *19*, 1366.

(52) Zhang, F.; Mi, W.; Wang, X. Spin-dependent electronic structure and magnetic anisotropy of 2D ferromagnetic janus $Cr_2I_3X_3$ (X = Br, Cl) monolayers. *Adv. Electron. Mater.* **2019**, *6*, 1900778.

(53) Zhang, F.; Zhang, H.; Mi, W.; Wang, X. Electronic structure, magnetic anisotropy and dzyaloshinskii−moriya interaction in janus $Cr_2I_3X_3$ (X = Br, Cl) bilayers. *Phys. Chem. Chem. Phys.* **2020**, *22*, 8647.

(54) Ren, Y.; Li, Q.; Wan, W.; Liu, Y.; Ge, Y. High-temperature ferromagnetic semiconductors: Janus monolayer vanadium trihalides. *Phys. Rev. B* **2020**, *101*, 134421.

(55) Lu, A.-Y.; Zhu, H.; Xiao, J.; Chuu, C.-P.; Han, Y.; Chiu, M.-H.; Cheng, C.-C.; Yang, C.-W.; Wei, K.-H.; Yang, Y.; et al. Janus monolayers of transition metal dichalcogenides. *Nat. Nanotechnol.* **2017**, *12*, 744−749.

(56) Zhang, J.; Jia, S.; Kholmanov, I.; Dong, L.; Er, D.; Chen, W.; Guo, H.; Jin, Z.; Shenoy, V. B.; Shi, L.; et al. Janus monolayer transition-metal dichalcogenides. *ACS Nano* **2017**, *11*, 8192−8198.

(57) Ma, Y.; Kou, L.; Huang, B.; Dai, Y.; Heine, T. Two-dimensional ferroelastic topological insulators in single-layer Janus transition metal dichalcogenides MSSe(M=Mo,W). *Phys. Rev. B* **2018**, *98*, 085420.

(58) Er, D.; Ye, H.; Frey, N. C.; Kumar, H.; Lou, J.; Shenoy, V. B. Prediction of enhanced catalytic activity for hydrogen evolution reaction in Janus transition metal dichalcogenides. *Nano Lett.* **2018**, *18*, 3943−3949.

(59) Kresse, G.; Hafner, J. Ab initiomolecular dynamics for liquid metals. *Phys. Rev. B: Condens. Matter Mater. Phys.* **1993**, *47*, 558−561.

(60) Kresse, G.; Furthmüller, J. Efficient iterative schemes forab initiototal-energy calculations using a plane-wave basis set. *Phys. Rev. B: Condens. Matter Mater. Phys.* **1996**, *54*, 11169−11186.

(61) Blöchl, P. E. Projector augmented-wave method. *Phys. Rev. B: Condens. Matter Mater. Phys.* **1994**, *50*, 17953−17979.

(62) Perdew, J. P.; Burke, K.; Ernzerhof, M. Generalized gradient approximation made simple. *Phys. Rev. Lett.* **1996**, *77*, 3865−3868.

(63) Monkhorst, H. J.; Pack, J. D. Special points for brillouin-zone integrations. *Phys. Rev. B: Solid State* **1976**, *13*, 5188−5192.

(64) Togo, A.; Tanaka, I. First principles phonon calculations in materials science. *Scr. Mater.* **2015**, *108*, 1−5.

(65) Bertolazzi, S.; Brivio, J.; Kis, A. Stretching and Breaking of Ultrathin MoS_2. *ACS Nano* **2011**, *5*, 9703−9709.

(66) Politano, A.; Chiarello, G. Probing the Young's modulus and Poisson's ratio in graphene/metal interfaces and graphite: a comparative study. *Nano Res.* **2015**, *8*, 1847−1856.

(67) Lee, C.; Wei, X.; Kysar, J. W.; Hone, J. Measurement of the elastic properties and intrinsic strength of monolayer graphene. *Science* **2008**, *321*, 385.

(68) Liechtenstein, A. I.; Katsnelson, M. I.; Antropov, V. P.; Gubanov, V. A. Local spin density functional approach to the theory of exchange interactions in ferromagnetic metals and alloys. *J. Magn. Magn. Mater.* **1987**, *67*, 65−74.

(69) Sivadas, N.; Daniels, M. W.; Swendsen, R. H.; Okamoto, S.; Xiao, D. Magnetic ground state of semiconducting transition-metal trichalcogenide monolayers. *Phys. Rev. B: Condens. Matter Mater. Phys.* **2015**, *91*, 235425.

(70) Xiang, H.; Lee, C.; Koo, H.-J.; Gong, X.; Whangbo, M.-H. Magnetic properties and energy-mapping analysis. *Dalton Trans.* **2013**, *42*, 823−853.

(71) Xu, C.; Feng, J.; Xiang, H.; Bellaiche, L. Interplay between kitaev interaction and single ion anisotropy in ferromagnetic CrI_3 and $CrGeTe_3$ monolayers. *npj Comput. Mater.* **2018**, *4*, 57.

(72) Wang, D.-s.; Wu, R.; Freeman, A. J. First-principles theory of surface magnetocrystalline anisotropy and the diatomic-pair model. *Phys. Rev. B: Condens. Matter Mater. Phys.* **1993**, *47*, 14932−14947.

(73) Yang, B. S.; Zhang, J.; Jiang, L. N.; Chen, W. Z.; Tang, P.; Zhang, X.-G.; Yan, Y.; Han, X. F. Strain induced enhancement of perpendicular magnetic anisotropy in Co/graphene and Co/BN heterostructures. *Phys. Rev. B* **2017**, *95*, 174424.

https://dx.doi.org/10.1021/acs.jpcc.0c04813